Article

Journal of
Nanoscience and Nanotechnology
Vol. 17, 7729–7734, 2017
www.aspbs.com/jnn

Copyright © 2017 American Scientific Publishers
All rights reserved
Printed in the United States of America

Corn Stem-Derived, Hierarchically Nanoporous Carbon as Electrode Material for Supercapacitors

Min Eui Lee[1], Jun Ho Choe[1], Young Soo Yun[2,*], and Hyoung-Joon Jin[1,*]

[1] Department of Polymer Science and Engineering, Inha University, Incheon 402-751, Republic of Korea
[2] Department of Chemical Engineering, Kangwon National University, Samcheok 245-711, Republic of Korea

Waste biomass-derived, carbon-based materials have potential as electrode materials for energy storage because of their advantageous characteristics, which include their low cost, sustainability, eco-friendly recycling, and intrinsic microstructures. In this study, corn stem-derived, hierarchically nanoporous carbon (CS-HNPC) was fabricated by carbonization of corn stems, followed by activation with potassium hydroxide. The CS-HNPC had a high specific surface area of ~1,420 m^2 g^{-1} and abundant nanopores with a hierarchical pore structure, which allowed the facile diffusion of electrolyte ions. It also showed a high specific capacitance of 232 F g^{-1} and good rate capabilities in an aqueous electrolyte when used as an electrode material for a supercapacitor. In addition, it exhibited stable cycling over 10,000 charge/discharge cycles at a current density of 10 A g^{-1}.

Keywords: Biomass, Corn Stems, Hierarchically Nanoporous Carbon, Electrode, Supercapacitor.

IP: 127.0.0.1 On: Mon, 25 May 2020 04:25:52
Copyright: American Scientific Publishers
Delivered by Ingenta

1. INTRODUCTION

Depletion of fossil fuel resources and increasing environmental concerns have attracted substantial attention to the development of sustainable power sources for various applications in the modern society.[1–3] Supercapacitors are rechargeable energy storage systems and are potential power sources because of their high power density and long cycling life.[4–7] However, the low energy density of supercapacitors—related to their charge-storage mechanism—hinders their broad applications. While rechargeable batteries can store a charge in the bulk host structures of their active electrode materials by redox reactions, supercapacitors do so by physical adsorption on and desorption from the electrode surface. Therefore, effective design of the electrode materials is very important to increase the energy density of supercapacitors. Nanoporous carbon materials have been widely studied as electrode materials for supercapacitors[8–12] since they have high specific surface areas, good electrical conductivities, and effective pore structures for charge storage. Waste biomass-derived nanoporous carbon materials also have additional advantages: they are inexpensive and renewable resources, and the generation of carbon materials is an eco-friendly recycling process for waste biomass.[13–15] Several reports have described the use of different types of waste biomass such as citrus peels, waste coffee grounds, dead leaves, seaweed, human hair, and pomelo shells to produce electrode materials for supercapacitors in the past few years.[16–20] The high specific surface area of the activated carbon materials obtained from waste coffee grounds and citrus peels was 1,945 and 1,167 m^2 g^{-1}, respectively, and these materials contained abundant pores. Additionally, waste coffee ground-based carbon electrodes were found to exhibit a high capacitance of 121 F g^{-1} in an organic electrolyte, along with a capacitance retention of 90.5% over 5,000 cycles.[17] Herein, we report the fabrication of nanoporous carbon materials from corn stems, which are one of the most abundant sources of waste biomass, with 170 to 256 million dry tons produced per year worldwide.[21] Through a simple pyrolysis process, corn stems were transformed into a nanoporous carbon material (corn stem-based carbon, CS-C). Moreover, we report the preparation of corn stem-based, hierarchically nanoporous carbon (CS-HNPC) by further development of the material's pore structure through chemical activation using potassium hydroxide. These CS-HNPC electrodes demonstrated superior electrochemical performance with a high specific capacitance and rate capability, as well as cycling stability.

*Authors to whom correspondence should be addressed.

2. EXPERIMENTAL DETAILS

2.1. Preparation of CS-C

The corn stems were obtained from a farm in Kangwon province, Republic of Korea. First, the corn stems were washed using distilled water and ethanol (99.9%, OCI Co, USA), dried in a vacuum oven at room temperature, and ground in a mixer to generate a powder. The resulting powder was thermally treated in a tube furnace by heating from room temperature to 800 °C over 2 h at a rate of 10 °C min^{-1} with a nitrogen flow rate of 300 mL min^{-1}.

2.2. Preparation of CS-HNPC

The CS-C was mixed with potassium hydroxide (Sigma-Aldrich, 98%, KOH) in a weight ratio of 0.5:1 (KOH: CS-C). The mixed sample was carbonized by heating to 800 °C under the same conditions. The CS-HNPC was washed with distilled water/ethanol and then dried in a vacuum oven at 60 °C.

2.3. Characterization

The morphologies were observed using field-emission scanning electron microscopy (FE-SEM, S-4300SE, Hitachi, Japan). The porosities and specific surface areas of the samples were analyzed based on nitrogen-adsorption and desorption isotherms obtained at −196 °C using the surface area and a porosimetry analyzer (ASAP 2020, Micromeritics, USA). The Brunauer-Emmett-Teller (BET) (S_{BET}) values were calculated according to the BET theory. The micropore surface area (S_{mic}) was determined using the t-plot theory, and the mesopore surface area (S_{meso}) was calculated according to the Barrett-Joyner-Halenda theory. Raman spectra were measured using a continuous-wave, linearly polarized laser (with a wavelength of 514.4 nm, 2.41 eV, and 16 mW of power). The laser beam was focused using a 100× objective lens, resulting in a spot with a diameter of ∼1 μm. The acquisition time and number of circulations used to collect each spectrum were 10 s and 3, respectively. An X-ray diffraction (XRD, Rigaku DMAX-2500) analysis of the samples was performed using Cu Kα radiation (wavelength $\lambda = 0.154$ nm) at 40 kV and 100 mA. The chemical compositions of the samples were examined using X-ray photoelectron spectroscopy (XPS, AXIS-HIS, Kratos Analytical, Japan) with monochromated Mg Kα radiation ($hv = 1500$ eV).

2.4. Electrochemical Characterization

The CS-HNPC-based electrodes for supercapacitors were prepared by loading a slurry consisting of 70 wt% active material, 20 wt% conductive carbon, and 10 wt% polytetrafluoroethylene (Sigma-Aldrich, 60 wt% dispersion in water, PTFE) on nickel forms, followed by drying at 80 °C for 2 h. The electrolyte was 6 M aqueous KOH. The electrochemical measurements were performed using cyclic voltammogram (CV), galvanostatic charge/discharge experiments, and electrical impedance spectroscopy (EIS) (PGSTAT302N, Metrohm Autolab, Netherlands). CV was performed using a three-electrode cell, in which a platinum wire was used as the counter electrode, the slurry material on the nickel form was the working electrode, and Ag/AgCl was the reference electrode in the potential range of −1 to 0 V at a scan rate of 40 mV s^{-1}. Galvanostatic charge/discharge measurements were performed at 1 A g^{-1} over a voltage range of −1 to 0 V versus Ag/AgCl. The cycling stability was evaluated by performing galvanostatic cycling between −1 and 0 V at 10 A g^{-1}. EIS was performed at the open-circuit voltage in the frequency range of 100–0.1 Hz.

3. RESULTS AND DISCUSSION

The morphologies of the CS-C and CS-HNPC were observed using SEM (Fig. 1). As shown in Figures 1(a) and (b), the morphologies are similar, and the magnified SEM images of the CS-HNPC reveal numerous macropores with diameters of several hundred nanometers in the inner walls of the bulk particles (Figs. 1(c) and (d)). These porous structures could have originated from the original corn stems. The fine pore structures of the CS-C and CS-HNPC were characterized by nitrogen-adsorption and desorption experiments. The nitrogen-adsorption and desorption isotherms of both samples resemble International Union of Pure and Applied Chemistry (IUPAC) type I, indicating microporous structures (Fig. 2(a)). The BET specific surface area of the CS-C was 865 m^2 g^{-1}, and most of the micropores were less than ∼2 nm in size (Fig. 2(b)). In contrast, the specific surface area of the CS-HNPC was higher: 1,420 m^2 g^{-1}. Additionally, the pore size distribution data of the CS-HNPC revealed that it had a considerable number of mesopores in the range of 2–20 nm and was dominated by micropores (Fig. 2(b)). Furthermore, the micropore and mesopore volumes gradually increased as the amount of activation agent increased. Other specific textural properties of these materials are summarized in Table I. The microstructures of the CS-C and CS-HNPC were examined using XRD and Raman spectroscopy, as shown in Figure 3. The diffraction pattern of the CS-C contains a broad peak at 23.5°, which is assigned to the graphite (002) plane, indicating a layered carbon structure (Fig. 3(a)). The diffraction pattern of the CS-HNPC exhibits a similar (002) peak, although it is broader. These data indicate that the CS-C and CS-HNPC have amorphous carbon structures with poor graphite stacking ordering. The Raman spectra of both samples exhibit D and G bands at ∼1,348 and ∼1,580 cm^{-1}, respectively (Fig. 3(b)). The D band is related to the vibration of carbon atoms with dangling bonds in the termination plane of disordered graphite, and the G band is associated with sp^2-carbon atoms in a hexagonal carbon structure. The intensity ratios (I_D/I_G) of the CS-C and CS-HNPC were calculated to be ∼0.95 and ∼1.73, respectively. These results demonstrate that the hexagonal carbon

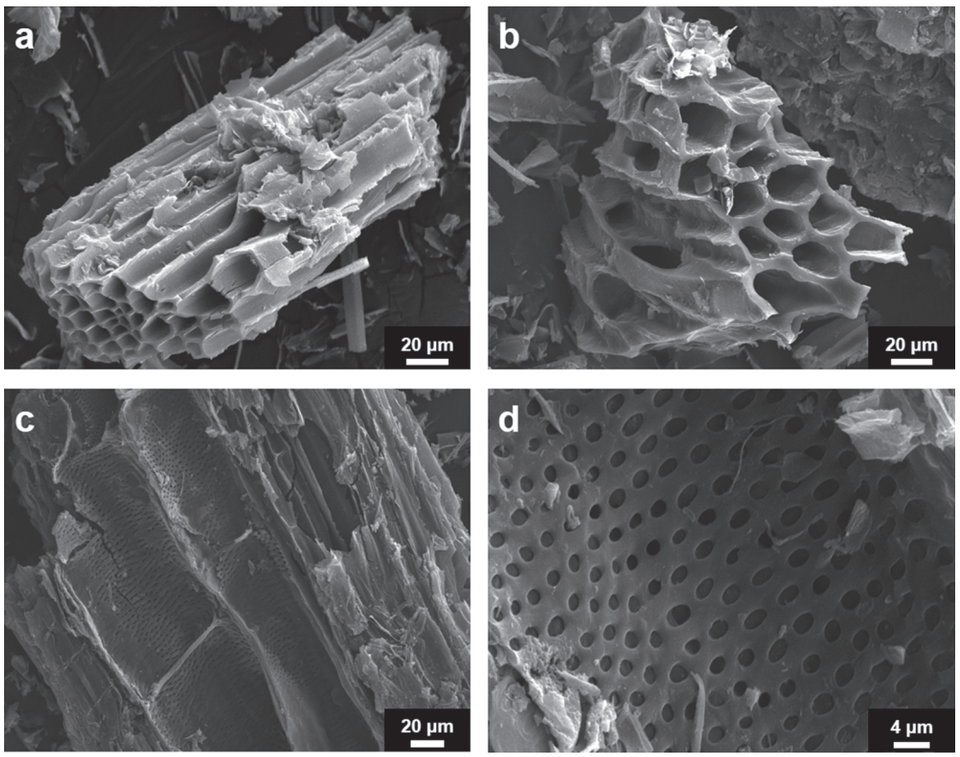

Figure 1. FE-SEM images of (a) CS-Cs and (b–c) CS-HNPCs and (d) high-magnification FE-SEM image of interior of CS-HNPCs shown in (c), revealing porous structure.

IP: 127.0.0.1 On: Mon, 25 May 2020 04:25:52
Copyright: American Scientific Publishers
Delivered by Ingenta

structure is several nanometers in size, and the amorphous carbon structure of the CS-HNPC is composed of numerous nanometer-sized crystallites with random orientations. These results correspond to the carbon structure of typical activated carbon, which contains a certain two-dimensional order but no three-dimensional graphitic ordering.[22–25] The surface properties of the CS-C and CS-HNPC were characterized by XPS (Fig. 4). In the C 1*s* spectra, C–O bonding (285.1 eV for CS-C; 285.8 eV for CS-HNPC) and C═O bonding (288.6 eV for CS-C; 288.0 eV for CS-HNPC) were observed, as well as a main C–C bonding peak centered at 284.3 eV, as shown in Figure 4(a). The O 1*s* spectra also show two distinct peaks: a C═O bonding peak centered at 531.0 eV and C–O bonding peaks centered at 531.9 and 532.3 eV for the CS-HNPC and CS-C, respectively (Fig. 4(b)). The C/O ratios of the CS-C and CS-HNPC were 4.5 and 7.6, respectively, confirming that the relative oxygen content of the CS-HNPC was reduced relative to that of the CS-C. This difference could be attributable to the emission of oxygen-containing compounds such as carbon dioxide during the activation process. The electrochemical performance of the CS-C- and CS-HNPC-based electrodes was investigated in 6 M aqueous KOH electrolyte over a potential range of −1 to 0 V

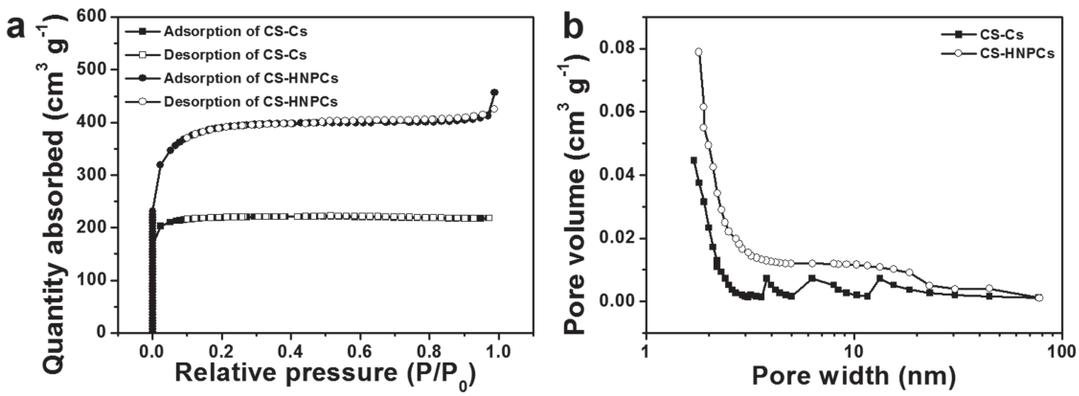

Figure 2. (a) Nitrogen-adsorption and desorption isotherm curves and (b) pore size distributions of CS-Cs and CS-HNPCs.

Table I. Specific textural properties of CS-Cs and CS-HNPCs.

Sample	S_{BET} (m^2 g^{-1})	S_{mic} (m^2 g^{-1})	V_{total} (cm^3g^{-1})	V_{mic} (cm^3g^{-1})	Average pore size (nm)	C/O ratio
CS-Cs	865	716	0.5	0.2	2.3	4.5
CS-HNPCs	1420	874	0.7	0.4	4.6	7.6

versus Ag/AgCl (Fig. 5). The CV curves of the CS-HNPC obtained at a scan rate of 40 mV s^{-1} exhibits a rectangular-like shape, indicating a capacitive charge-storage behavior (Fig. 5(a)). The steep slopes of the current change at the switching potentials reflect a small mass-transfer resistance. In contrast, the CV curves of the CS-C show a relatively dented shape compared to that of the CS-HNPC, and its overall area is smaller than that of the CS-HNPC's CV. These data indicate that the CS-HNPC has a superior charge storage performance, possibly resulting from its higher specific surface area and hierarchical pore structure. The galvanostatic charge/discharge profiles of the CS-C and CS-HNPC show an isosceles triangle shape, in good agreement with the CV results (Fig. 5(b)). The discharge time of the CS-HNPC was noticeably longer than that of the CS-C at the same current density (1 A g^{-1}); thus, the CS-HNPC has a larger capacitance than the CS-C. The specific capacitances of the CS-HNPC and CS-C were calculated to be 254 and 148 F g^{-1}, respectively, at a current density of 0.4 A g^{-1} (Fig. 5(c)). The capacitance values gradually decreased as the current density increased. At current densities of 1, 4, and 10 A g^{-1}, the specific capacitances of the CS-HNPC were 232, 199, and 169 F g^{-1}, respectively. When the current density was 25 times higher, specific capacitance values of approximately 67% were maintained, indicating that the CS-HNPC had good rate capabilities. For the CS-C, specific capacitances of 136, 115, and 92 F g^{-1} were recorded at current densities of 1, 4, and 10 A g^{-1}, respectively. For all the current densities tested, the capacitance values of the CS-C were much smaller than those of the CS-HNPC. These materials' good rate performances were further illustrated by their Nyquist plots in the frequency range of 100 kHz to 0.1 Hz, as shown in Figure 5(d). These plots feature vertical lines in the low-frequency region, indicating an ideal capacitive behavior. The equivalent series resistance (ESR) of the CS-HNPC was 2.8 Ω, which was smaller than that of the CS-C (3.3 Ω), suggesting that the CS-HNPC had fast charge-storage kinetics. In addition, the CS-HNPC-based supercapacitors exhibited stable cycling

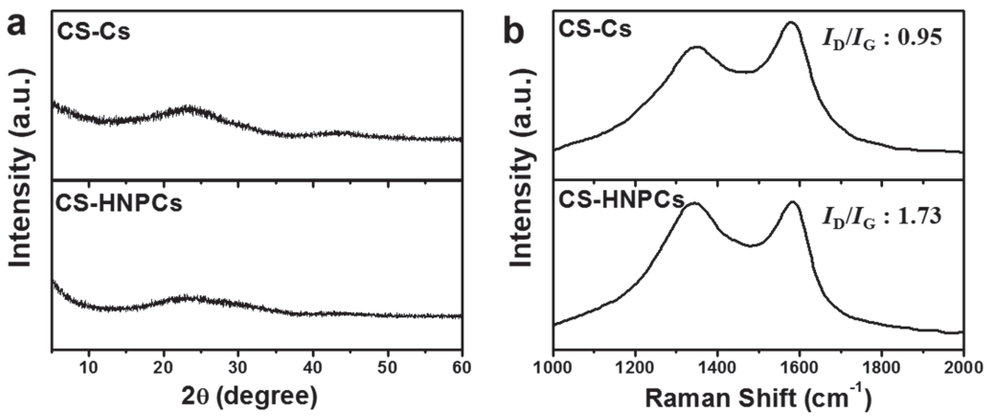

Figure 3. (a) XRD patterns and (b) Raman spectra of CS-Cs and CS-HNPCs.

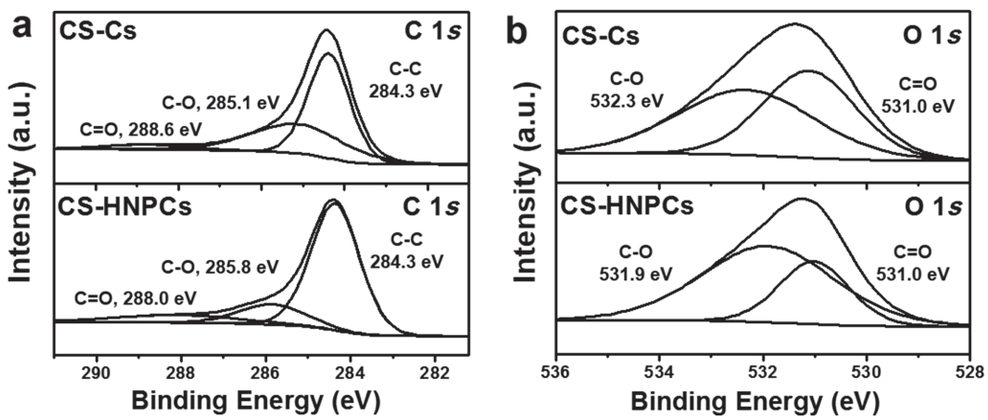

Figure 4. XPS (a) C 1*s* and (b) O 1*s* spectra of CS-Cs and CS-HNPCs revealing various chemical configurations.

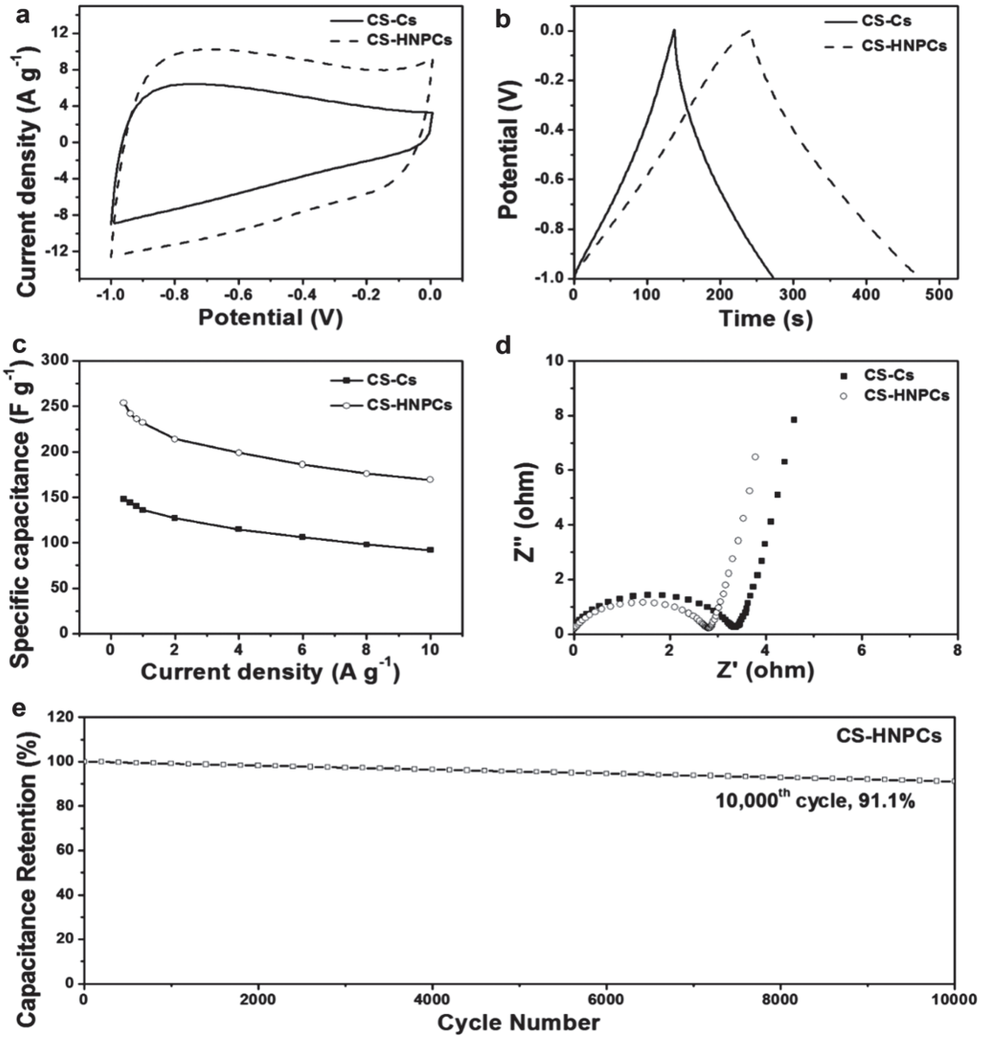

Figure 5. Electrochemical performances over potential range of −1 to 0 V in aqueous KOH electrolyte: (a) CV curves of CS-C- and CS-HNPC-based supercapacitors at scan rate of 40 mV s^{-1}, (b) galvanostatic charge/discharge curves of CS-C- and CS-HNPC-based supercapacitors at current density of 1 A g^{-1}, (c) specific capacitances of supercapacitors based on CS-C and CS-HNPC measured at various current densities, (d) Nyquist plots of CS-C- and CS-HNPC-based supercapacitors over frequency range of 100–0.1 Hz, and (e) capacitance retention of CS-HNPC-based supercapacitors over 10,000 charge/discharge cycles at current density of 1 A g^{-1}.

over 10,000 charge/discharge cycles at a current density of 1 A g^{-1} (Fig. 5(e)). Furthermore, a capacitance retention of 91.1% was achieved after 10,000 cycles.

4. CONCLUSIONS

In summary, CS-HNPC was fabricated via the carbonization of corn stems, followed by KOH activation. The CS-HNPC had a higher specific surface area and larger, nanometer-scale pores than the CS-C, which was prepared by the carbonization of corn stems without chemical activation. The CS-HNPC had a specific surface area of 1,420 m^2 g^{-1}, numerous nanopores, and mesopores with diameters of 2–20 nm originating from a defective carbon structure with poor graphite stacking ordering. The CS-HNPC also had a C/O ratio of 7.6, indicating the presence of oxygen heteroatoms. As an electrode material for supercapacitors, the CS-HNPC showed a high specific capacitance of 232 F g^{-1}, good rate capabilities at a current density of 10 A g^{-1}, and a stable capacitance retention of 91.1% over 10,000 cycles.

Acknowledgment: This work was supported by an Inha University Research Grant (2017).

References and Notes

1. Y. S. Yun, K.-Y. Park, B. Lee, S. Y. Cho, Y.-U. Park, S. J. Hong, B. H. Kim, H. Gwon, H. Kim, S. Lee, Y. W. Park, H.-J. Jin, and K. Kang, *Adv. Mater.* 27, 6914 (**2015**).
2. X. Du, L. Wang, W. Zhao, Y. Wang, T. Qi, and C. M. Li, *J. Power Sources* 323, 166 (**2016**).
3. P. Kumar and K.-H. Kim, *Appl. Energy* 172, 383 (**2016**).

4. P. Simon and Y. Gogotsi, *Nat. Mater.* 7, 845 (**2008**).
5. A. G. Pandolfo and A. F. Hollenkamp, *J. Power Sources* 157, 11 (**2006**).
6. L. L. Zhang and X. S. Zhao, *Chem. Soc. Rev.* 38, 2520 (**2009**).
7. Y. Zhu, S. Murali, M. D. Stoller, K. J. Ganesh, W. Cai, P. J. Ferreira, A. Pirkle, R. M. Wallace, K. A. Cychosz, M. Thommes, D. Su, E. A. Stach, and R. S. Ruoff, *Science* 332, 1537 (**2011**).
8. Y. S. Yun, S. Y. Cho, J. Shim, B. H. Kim, S.-J. Chang, S. J. Baek, Y. S. Huh, Y. Tak, Y. W. Park, S. Park, and H.-J. Jin, *Adv. Mater.* 25, 1993 (**2013**).
9. W.-G. Jo, M. Khan, L.-S. Tan, H.-S. Jeong, S.-H. Lee, and S.-Y. Park, *Macromol. Res.* 25, 335 (**2017**).
10. Y. S. Yun, C. Im, H. H. Park, I. Hwang, Y. Tak, and H.-J. Jin, *J. Power Sources* 234, 285 (**2013**).
11. L. Yao, G. Yang, P. Han, Z. Tang, and J. Yang, *J. Power Sources* 315, 209 (**2016**).
12. H. Li, D. Yuan, C. Tang, S. Wang, J. Sun, Z. Li, T. Tang, F. Wang, H. Gong, and C. He, *Carbon* 100, 151 (**2016**).
13. P. Chen, L.-K. Wang, G. Wang, M.-R. Gao, J. Ge, W.-J. Yuan, Y.-H. Shen, A.-J. Xie, and S.-H. Yu, *Energy Environ. Sci.* 7, 4095 (**2014**).
14. G. Hegde, S. A. A. Manaf, A. Kumar, G. A. M. Ali, K. F. Chong, Z. Ngaini, and K. V. Sharma, *ACS Sustainable Chem. Eng.* 3, 2247 (**2015**).
15. J. Li and Q. Wu, *New J. Chem.* 39, 3859 (**2015**).
16. N. R. Kim, Y. S. Yun, M. Y. Song, S. J. Hong, M. Kang, C. Leal, Y. W. Park, and H.-J. Jin, *ACS Appl. Mater. Interfaces* 8, 3175 (**2016**).
17. Y. S. Yun, M. H. Park, S. J. Hong, M. E. Lee, Y. W. Park, and H.-J. Jin, *ACS Appl. Mater. Interfaces* 7, 3684 (**2015**).
18. M. Biswal, A. Banerjee, M. Deo, and S. Ogale, *Energy Environ. Sci.* 6, 1249 (**2013**).
19. E. Raymundo-Piñero, M. Cadek, and F. Béguin, *Adv. Funct. Mater.* 19, 1032 (**2009**).
20. W. Qian, F. Sun, Y. Xu, L. Qiu, C. Liu, S. Wang, and F. Yan, *Energy Environ. Sci.* 7, 379 (**2014**).
21. K. B. Cantrell, J. M. Novak, J. R. Frederick, D. L. Karlen, and D. W. Watts, *Bioenerg. Res.* 7, 590 (**2014**).
22. Y. S. Yun, S. Lee, N. R. Kim, M. Kang, C. Leal, K.-Y. Park, K. Kang, and H.-J. Jin, *J. Power Sources* 313, 142 (**2016**).
23. Y. S. Yun, S. Y. Cho, H. Kim, H.-J. Jin, and K. Kang, *ChemElectroChem.* 2, 359 (**2015**).
24. Y. S. Yun, G. Yoon, K. Kang, and H.-J. Jin, *Carbon* 80, 246 (**2014**).
25. Y. S. Yun, M. E. Lee, M. J. Joo, and H.-J. Jin, *J. Power Sources* 246, 540 (**2014**).

Received: 3 August 2016. Accepted: 27 February 2017.

IP: 127.0.0.1 On: Mon, 25 May 2020 04:25:52
Copyright: American Scientific Publishers
Delivered by Ingenta